Comparative Target Analysis of Chlorinated Biphenyl Antimicrobials Highlights MenG as Molecular Target of Triclocarban

Robert Macsics[a], Mathias W. Hackl[a], Christian Fetzer[a], Dietrich Mostert[a], Jennifer Bender[b], Franziska Layer[b], Stephan A. Sieber[a,c]#

[a]Chair of Organic Chemistry II, Technische Universität München, Garching bei München, Germany.

[b]National Reference Centre for Staphylococci and Enterococci, Robert Koch Institute, Wernigerode, Germany.

[c]Helmholtz Institute for Pharmaceutical Research Saarland, Helmholtz Centre for Infection Research, Saarbrücken, Germany.

#Corresponding author: stephan.sieber@tum.de

Running title: Target Analysis of Chlorinated Biphenyl Antimicrobials

Abstract

Triclocarban (TCC), a formerly used disinfectant, kills bacteria via an unknown mechanism of action. A structural hallmark is its *N,N'*-diaryl urea motif which is also present in other antibiotics including the recently reported small molecule PK150. We here show that, like PK150, TCC exhibits an inhibitory effect on *Staphylococcus aureus* menaquinone metabolism via inhibition of the biosynthesis protein MenG. However, the activity spectrum (MIC_{90}) of TCC across a broad range of multi-drug resistant

staphylococci and enterococci strains was much narrower compared to PK150. Accordingly, TCC did not cause an over-activation of signal peptidase SpsB, a hallmark of the PK150 mode of action. Furthermore, we were able to rule out inhibition of FabI, a confirmed target of the diaryl ether antibiotic triclosan (TCS). Differences in the target profile of TCC and TCS were further investigated by proteomic analysis, showing complex, but rather distinct changes in the protein expression profile of *S. aureus*. Downregulation of the arginine deiminase pathway provided additional evidence for an effect on bacterial energy metabolism by TCC.

Importance

TCC's widespread use as an antimicrobial agent has made it a ubiquitous environmental pollutant despite its withdrawal due to ecological and toxicological concerns. With its antibacterial mechanism of action still being unknown, we undertook a comparative target analysis between TCC, PK150, a recently discovered antibacterial compound with structural reminiscence to TCC, and TCS, another widely employed chlorinated biphenyl antimicrobial, in the bacterium *Staphylococcus aureus*. We show that there are distinct differences in each compound's mode of action, but also identify a shared target between TCC and PK150, which is interference with menaquinone metabolism by inhibition of MenG. The prevailing differences, however, which also manifest in a remarkably better broad spectrum activity of PK150, suggest that even high levels of TCC or TCS resistance observed by continuous environmental exposure may not affect the potential of PK150 or related *N,N'*-diaryl urea compounds as new antibiotic drug candidates against multi-drug resistant infections.

Introduction

Triclocarban (TCC) is a broad-spectrum anti-infective agent that has been used in personal care products such as soaps and lotions since the 1960s (1). In 2017, however, the Food and Drug Administration (FDA) banned the use of TCC together with triclosan (TCS), another halogenated biphenyl antimicrobial agent (Fig. 1), because of safety concerns. TCC and TCS can be absorbed by the body (2,3) and were found to interfere with several mammalian off-targets: both act as weak endocrine disruptors (4); TCC was additionally found to exhibit anti-inflammatory effects by inhibiting soluble epoxide hydrolase and to alter cardiac function by interference with fatty acid metabolism in murine mouse models (3, 5, 6). TCS, in contrast, was demonstrated to depolarize the inner mitochondrial membrane and uncouple oxidative phosphorylation (7–9). Adding to these health-related concerns are environmental problems: due to their multiple chlorination sites, these compounds are persistent to biodegradation, and were thus shown to accumulate in the environment and cause potentially toxic effects in soil and water organisms (10–15).

In contrast to the very extensive studies on its impact on health and environment, surprisingly little is known about the antibacterial mode of action of TCC. While TCS is known to inhibit enoyl-acyl-carrier-protein reductase FabI (16–18) and proposed to further disturb the lipid bilayer non-specifically at higher concentrations (19), the corresponding mechanisms for TCC are rather unclear and studies into their elucidation are scarce: one study investigated the production of membrane leakage by several compounds, but found no such effect for TCC (20). Comparison of TCC and TCS by molecular dynamics simulations, though, suggested that at high concentrations both

compounds might destabilize the lipid bilayer membrane in a similar non-specific manner (21). Finally, a study which aimed at generating improved derivatives of TCC investigated the mode of action by fluorescence staining and microscopy, and found TCC to induce cell lysis and membrane deformation (22). However, a specific protein target as in the case of TCS has not been identified so far.

Recently, we published the development of a novel antibacterial compound named PK150, which was derived from the anti-cancer drug sorafenib (SFN, Fig 1) (23). Extensive mode of action analysis validated two independent protein targets in *Staphylococcus aureus*, which involved the over-activation of signal peptidase Ib (SpsB), a key enzyme in the bacterial secretory pathway, and inhibition of demethylmenaquinone methyltransferase (MenG), the last step in the biosynthesis of the essential electron carrier menaquinone. Given the structural similarity between PK150 and TCC, including the characteristic *N,N'*-diaryl urea motif, it is well conceivable that some of these mechanistic features identified for PK150 might also apply to TCC. This is corroborated by some similarities which both compounds exert on target cells including membrane deformation and cell lysis (23). Additionally, both compounds are only active in Gram-positive bacteria and development of resistance has not yet been observed under laboratory conditions (23, 24).

In this work we show that the target profile of TCC exhibits similar but also distinct features compared to PK150. While MenG is inhibited by both compounds, we rule out a contribution of SpsB to TCC's mode of action. Furthermore, TCC does not inhibit FabI and also shows distinct differences to TCS in proteomic profiling. As such, this work underlines the versatility of *N,N'*-diaryl urea and diaryl ether antibiotics and proposes the contribution of a specific target to the overall mode of action of TCC.

Results

PK150 and TCC differ in their spectrum of activity against multi-drug resistant staphylococci and enterococci. We first analyzed whether the two *N,N'*-diaryl ureas PK150 and TCC exert a comparable activity profile against a variety of multi-drug resistant clinical strains, among them bacteria resistant to last resort antibiotics such as linezolid, vancomycin or daptomycin. We determined the minimal inhibitory concentration (MIC) of both compounds in 100 different staphylococci strains, mainly *S. aureus*, and 100 enterococci strains, mainly *E. faecium* and *E. faecalis*, to define the compound concentration at which the growth of at least 90% of strains is inhibited (MIC_{90}, Fig. 2 and Supplementary Data 1). We found the activity profile of both compounds to be very different: PK150 exhibited activity against all tested strains, with an MIC_{90} of 0.78 µM against staphylococci and an MIC_{90} of 3.13 µM against enterococci. In contrast, TCC showed a remarkably broad MIC distribution and was inactive against 17% of staphylococci and 89% of enterococci (MIC_{90} of >25 µM in both cases). This not only demonstrates that the antibacterial properties of PK150 are superior to TCC, but also suggests fundamental differences in their mode of action. We further looked into 40 staphylococci strains exhibiting intermediate or high level resistance against TCC ($MIC \geq 6.25$ µM), but could not observe any differences regarding their general resistance pattern compared to the full strain selection (Supplementary Data 1). However, we noted that none of those 40 strains belonged to the clonal complex subtype 5 ST225 (spa type t003; “Rhine-Hesse Epidemic strain”), which is one of the predominant hospital-associated MRSA in Germany, although 9% of our collection comprised this subtype (25, 26).

105 **TCC and TCS show little to no effect on bacterial membrane integrity.** We
106 next investigated the mechanistic reasons for these observed differences. First, we
107 looked into the effect of TCC on the general integrity of the bacterial cell membrane. As
108 mentioned above, evidence for induced membrane leakage was not found in previous
109 experiments, but TCC is predicted to perturb the membrane at higher concentrations
110 (20, 21). For our assay, we analyzed the interaction of the dye propidium iodide with
111 bacterial DNA, which is only accessible if the cell membrane is permeabilized. As a
112 positive control, the detergent benzalkonium chloride (27) was used and evoked an
113 immediate and drastic increase in fluorescence (Fig. 3A). PK150 was previously shown
114 to induce an increase in dye fluorescence, likely a consequence of autolysin induced cell
115 lysis (23), and a moderate, concentration-dependent effect was also observed here (Fig.
116 3A). Of note, the strain tested herein differs from the strain used in the previous study,
117 which could account for differences in total fluorescence increase. In contrast, TCC
118 induced a much weaker effect than PK150 and TCS shows no change compared to the
119 DMSO control at all (Fig. 3A). This confirms that both TCC and TCS do not act via
120 membrane perturbation at concentrations close to their MIC and further suggests the
121 existence of specific targets for TCC and TCS (where FabI is a known target).
122 **TCC does not overactivate PK150's target SpsB.** Given their structural
123 similarity, we next examined whether TCC interacts with the known targets of PK150.
124 One unprecedented property of PK150 is its capability to overactivate the signal
125 peptidase SpsB. This can be measured in a FRET-based peptidase assay using an
126 artificial fluorescent substrate and endogenous SpsB embedded into native membranes
127 of *S. aureus* (23). We performed this assay at three different concentrations of both TCC
128 and TCS and also added PK150 as positive control for an SpsB activator (Fig 3B). TCC

129 did not exhibit a stimulatory effect on SpsB activity, indicating an important mechanistic
130 difference to PK150. Interestingly, TCS induced a moderate activation of the enzyme,
131 despite its structure being more distant to PK150 compared to TCC.

132 **TCC inhibits PK150's other target MenG.** Regarding the second confirmed
133 cellular mechanism of PK150, inhibition of MenG, we examined whether addition of
134 menaquinone-4 (MK-4) rescued bacteria from TCC and TCS treatment. Interestingly, a
135 moderate shift of MIC up to about 6-fold, dependent on MK-4 concentration, was
136 observed (Fig. 4A) for both compounds. To exclude that unspecific effects, such as
137 aggregation of the compounds by high concentrations of MK-4 or a general fitness
138 increase of the cells (due to the additional vitamin supply), interfere with the assay and
139 contribute to these results, we performed further validation experiments: First, we
140 quantified endogenous levels of menaquinone-8 (MK-8) in live *S. aureus* cells treated
141 with TCC, TCS or ciprofloxacin as control. MK-8 levels were reduced in a concentration-
142 dependent manner by up to 47% by TCC and up to 29% by TCS on average, which was
143 not observed by ciprofloxacin treatment (Fig. 4B). Second, we measured MenG
144 inhibition directly by methylation of the artificial substrate demethylmenaquinone-2
145 (DMK-2) in lysates of *S. aureus* cells overexpressing MenG, extraction and subsequent
146 LC-MS analysis. Again, TCC showed stronger effects and reduced MenG activity by
147 23% at 5 µM compound concentration and up to 73% at 50 µM, while TCS inhibited
148 MenG only at a concentration of 50 µM and to an extent of 41% (Fig. 4C). PK150, in
149 comparison, had been shown to diminish endogenous MK-8 by up to 33% and to reduce
150 MenG activity by 70% at the same respective concentrations (23).

151 **Neither TCC nor PK150 inhibit TCS's target FabI.** Given the similarity between
152 TCS and TCC with regard to human off-targets and environmental behavior and the fact

153 that FabI is a confirmed target of TCS, we next investigated whether TCC might interact
154 with FabI in a similar manner. We cloned and purified *S. aureus* FabI and assayed its
155 activity on reducing trans-2-octenoyl *N*-acetylcysteamine thioester (*t*-o-NAC thioester), a
156 common artificial substrate for this enzyme (28). We were able to reproduce the
157 inhibition caused by TCS, while neither TCC nor PK150 exhibited a significant inhibitory
158 effect (Fig. 5).

159 **Full proteome analysis reveals different patterns for TCC and TCS**
160 **treatment.** In order to analyze the effects evoked by the compounds on a global level,
161 we performed whole proteome analysis of *S. aureus* cells treated with sub-inhibitory
162 concentrations (0.5 x MIC) of TCC or TCS (Fig. 6A,B, Supplementary Data 2). Bacterial
163 proteins were digested with trypsin and subjected to analysis by liquid chromatography-
164 tandem mass spectrometry following label free quantification of identified peptides (29).
165 Analysis of proteins whose expression levels were significantly altered between DMSO
166 and compound-treated condition (|log(protein ratio)| > 1 & -log(*P*-value) > 1) revealed
167 only one overlapping protein between TCC and TCS treatment (PTS system EIIBC
168 component, Q2G1G5), supporting the view that the underlying mechanisms of action
169 are rather distinct from each other (Fig. 6C). We further tried to identify particular
170 pathways that might be up- or downregulated by network analysis with STRING (Fig.
171 6A,B,D, Supplementary Data 2) (30). Most strikingly, a significant downregulation of the
172 entire arginine deiminase pathway (arginine deiminase (*arcA*, Q2FUX7), carbamate
173 kinase 1 (*arcC1*, Q2FZA9), carbamate kinase 2 (*arcC2*, Q7X2S2), and two ornithine
174 carbamoyltransferases (*arcB/argF*, Q2FUX8, and *argF*, Q2FZB0)) was observed upon
175 TCC treatment (Fig. 6D) (31). Regarding upregulated proteins, two proteins were found
176 to be generally associated with dicarboxylic acid metabolism by GO (32, 33) annotation

177 (Supplementary Data 2), but no significant interaction network was detected. For TCS
178 treatment, there was no significant pathway enrichment among upregulated proteins and
179 only a few downregulated proteins were found to be involved in functional enrichment,
180 which are associated with carbohydrate phosphotransferase activity or transmembrane
181 transport by GO (32, 33) and Pfam (34) annotation, but do not give rise to a
182 comprehensive pathway (for details see Supplementary Data 2).
183
184
185 **Discussion**
186
187 Overactivation of SpsB has been identified as a key feature of the PK150 scaffold,
188 leading to increased secretion of autolytic enzymes and subsequent cell lysis, but,
189 despite its structural similarity, we could not confirm the same activity for TCC. In
190 addition, TCC was inactive against most tested enterococci and also a good proportion
191 of staphylococci. Although the reasons for this observation might be complex and further
192 work is required for their exact elucidation, it seems plausible that the differences in
193 SpsB activation could contribute to these diverging effects. Furthermore, it indicates that
194 the mechanisms leading to TCC resistance do not affect susceptibility towards PK150,
195 suggesting that environmental exposure of bacteria to TCC is unlikely to evoke cross-
196 resistance against PK150 or related *N,N'*-diaryl ureas.
197 However, the shift of MIC in the presence of MK-4, the reduction of endogenous
198 menaquinone levels in live cells and the direct inhibition of MenG activity in cellular
199 lysate are comparable traits of both compounds (23). Based on these findings, it is well
200 conceivable that MenG inhibition is involved in TCC's mode of action, which points

towards it being the first ever identified molecular target of TCC. Of course, this does not exclude the existence of additional target mechanisms, which can include other proteins and in principle also non-specific effects such as membrane disruption. However, our finding that TCC barely affects membrane permeability, which is in accordance with its failure to induce potassium leakage in an earlier study (20), is contradictory to unspecific membrane damage and supports the view of a more specific mechanism.

Nevertheless, the proteomic data deliver a complex picture of the processes underlying TCC treatment. Of note, no effect on menaquinone metabolism was observed. Instead, the most significant finding was a downregulation of the arginine deiminase pathway. Interestingly, this pathway was found to be upregulated in the proteomes of *S. aureus* resistant to the PK150 parent compound SFN (23). The arginine deiminase pathway catabolizes arginine to carbamoyl phosphate, which is further converted to ammonia, carbon dioxide and ATP (31). It has been associated with enhanced fitness and virulence as the MRSA strain USA300 carries a mobile genetic element containing an additional arginine deiminase operon, which serves as an epidemiological marker (35). Importantly, it represents a way to generate energy which is independent of menaquinone (31). Thus, while its upregulation makes sense for cells resistant to a disruptor of menaquinone biosynthesis, it is rather surprising that the exact opposite is found in the case of TCC and non-resistant cells. Such a response would actually aggravate the detrimental consequences of MenG inhibition. Hence, although the exact mechanisms inducing these changes remain unclear, they appear to strengthen the antibiotic effect of TCC and also provide an independent link for alterations in bacterial energy metabolism.

Applied and Environmental Microbiology

The proteomic data further revealed a completely different picture in the case of TCS treatment. Unfortunately, the pattern of up- and downregulated proteins does not give rise to a clearly targeted pathway. Nevertheless, together with the finding that TCC does not inhibit FabI, these data suggest that both compounds act by different mechanisms.

An interesting finding is that TCS exhibits a stimulation of SpsB activity as well as an inhibitory effect on menaquinone biosynthesis. Both effects are only weak to moderate and comparable to what was observed with SFN, which is about ten times less potent than TCS (23). Of note, mutations in FabI, which are commonly referred to as conferring TCS resistance, do not produce fully resistant strains, but merely decrease the activity of TCS of about an order of magnitude (18, 36). In addition, similarly TCS-resistant bacteria have also been isolated which show no alterations in the *fabI* gene (36). It is thus not surprising that the involvement of other, unknown targets for the mode of action of TCS has been proposed before (37). Although further experiments are needed for validation, our experiments point to the possibility that SpsB and MenG could represent such additional targets, particularly at higher TCS concentrations.

Taken together, we identified MenG as a putative molecular target of TCC, reminiscent to structurally related PK150, but also established distinct differences between the two compounds as well as to TCS. Hence, our findings shed some light on the obscure mechanism of TCC and underline menaquinone biosynthesis inhibition as an important antibiotic target pathway. In addition, our work highlights the novelty of the PK150 structure as a promising entity with potential against multi-drug resistant pathogens, which is unlikely to be affected by environmentally acquired TCC resistance.

248 **Materials and Methods**

249 **Materials and strains.** TCC and TCS were purchased from *Sigma Aldrich*. MK-4 and
250 MK-9 were purchased from *Santa Cruz Biotechnology* and *Carbosynth*, respectively.
251 PK150 and DMK-2 were synthesized as reported previously (23). Unless otherwise
252 stated, *S. aureus* NCTC 8325 (Institute Pasteur, France) was used for laboratory
253 experiments and cultured in B medium (10 g/L casein peptone, 5 g/L NaCl, 5 g/L yeast
254 extract, 1 g/L K_2HPO_4, pH 7.5). The collection of staphylococci and enterococci for
255 MIC_{90} determination was provided by the National Reference Centre for Staphylococci
256 and Enterococci (Robert Koch Institute, Wernigerode, Germany). Further details on the
257 specific strains can be found in Supplementary Data 1.

258 **MIC determination, MIC_{90}, and MK-4 shift assay.** *Staphylococcus aureus* cultures
259 were grown at 37°C with gentle shaking (200 rpm) in B medium from overnight cultures
260 until OD_{600}~0.4–0.6, and diluted into B medium to give a final a concentration of
261 10^5 colony forming units (CFU)/mL. Compounds at various concentrations were added
262 to diluted bacterial cultures (100 µL/well final volume; final concentration of DMSO from
263 compound stocks 1%) in triplicates. A growth control containing DMSO only and a sterile
264 control containing medium were included. After incubation (37°C, 200 rpm, 24 h), the
265 dilution series was analyzed for microbial growth as indicated by turbidity. The lowest
266 concentration in the dilution series at which no growth of bacteria could be observed by
267 eye was defined as the minimum inhibitory concentration (MIC) of the compound. MIC
268 values were determined by three independent experiments. Note that for the case of
269 TCS the MIC in *S. aureus* NCTC 8325 was found to vary between 0.3 µM and 0.5 µM.
270 For experiments relating to this MIC, a value was determined beforehand and this same

271 value taken for the subsequent respective experiment. These values were: 0.3 µM for
272 metabolic menaquinone profiling (Fig. 4B) and full proteome analysis (Fig. 6), 0.39 µM
273 for membrane integrity assay (Fig. 3A), and 0.5 µM for MIC shift assay (Fig. 4A).

274 For MIC_{90} determination, clinical isolates were grown on Mueller-Hinton Broth (MHB)
275 culture plates and 3 to 4 single colonies were picked and used to inoculate 5 mL MHB.
276 Cultures were grown until they reached an optical density corresponding to 0.5
277 McFarland units. These cultures were diluted 1:50 in 0.85% (w/v) NaCl solution to
278 prepare the final inoculum. 1 µL of a 3 mM stock solution in DMSO of the respective test
279 compounds was placed in the first column of a round-bottom 96-well plate. The wells of
280 this column were filled up with 99 µL of MHB. Columns 2 to 12 were filled with 50 µL
281 MHB and two-fold serial dilutions of the test compounds were made by transferring 50
282 µL from column 1 to column 2 and so forth until column 10. Column 11 served as growth
283 control and column 12 as sterile control. The plate was inoculated by adding 10 µL of
284 the freshly prepared inoculum to the wells of column 1 through 11. Bacteria were grown
285 at 37 °C for 20 h without agitation. The MIC was determined as the lowest compound
286 concentration with no observable bacterial growth after visual inspection. All MIC raw
287 data and information on the characteristics of the tested strains have been uploaded to
288 the supplementary information as an Excel file (Supplementary Data 1).

289 For MIC shift assays in the presence of exogenous menaquinone-4 (MK-4), the growth
290 medium was additionally supplemented with different concentrations of MK-4 before
291 addition of the bacteria, giving a total DMSO concentration in the final assay of 1.5%.

292 **Membrane Integrity assay.** To asses cell wall permeability upon treatment with
293 compounds, cells (*S. aureus* NCTC 8325) were grown (37°C, 200 rpm) from a

294 respective over-night culture until they reached an OD_{600} value of 0.4–0.8. The cells
295 were then harvested (6000 x g, 4°C, 5 min), washed with 5 mM HEPES-NaOH buffer
296 (pH 7.2 supplemented with 5 mM glucose) and then resuspended in the same buffer to
297 an OD_{600} of 0.4. The assay was conducted in 96-well plates (Nunc flat-bottom
298 transparent 96-well plates, *Thermo Fischer Scientific*) with 99 µL cell-suspension per
299 well. The assay was started by adding 1 µL of 1 mM propidium iodide (*Sigma-Aldrich*) in
300 DMF to each well (10 µM final concentration) and incubating at 37°C in the *TECAN*
301 Infinite M200 Pro microplate reader to allow the propidium iodide to be integrated into
302 the membranes. During incubation, fluorescence was measured (535 nm excitation and
303 617 nm emission). After 15 min, 1 µL of the respective compound or control was added
304 from DMSO stocks with the appropriate concentrations to each well. The fluorescence
305 was measured for 60 min at 37°C. As a positive control, 16 µg/mL (8-fold MIC) of the
306 detergent benzalkonium chloride (BAC) was added to the cell suspension, while 1 µL
307 DMSO was added for a baseline fluorescence control.

308 **FRET-based SpsB activity assay.** SpsB activities were measured using membranes of
309 *S. aureus* and a Förster Resonance Energy Transfer (FRET) assay as described
310 previously (23, 38). Briefly, *S. aureus* NCTC 8325 membranes containing native SpsB
311 (0.2 mg/mL total protein concentration) were pretreated with different concentrations of
312 compound (TCC, TCS, and positive control PK150) or DMSO for 5 min at 37°C. A
313 synthetic peptide substrate based on SceD modified by 4-(4-
314 dimethylaminophenylazo)benzoic (DABCYL) acid and 5-((2-aminoethyl)amino)-1-
315 naphthalenesulfonic acid (EDANS) was added (DABCYL-AGHDAHASET-EDANS,
316 *AnaSpec*) to give 10 µM final substrate concentration (1:100 from DMF stock) and
317 fluorescence was monitored by a *Tecan* Infinite 200Pro plate reader for 1 h at 37°C

(345 nm excitation and 510 nm emission wavelength). SpsB activity was determined by the slope of the fluorescence increase and normalized to the DMSO control.

Metabolic profiling of endogenous MK-8. The experiments were performed as described previously (23). Mid-exponential phase cultures of S. aureus NCTC 8325 were diluted into B medium to give a final concentration of 10^5 CFU/mL. TCC, TCS and control ciprofloxacin (Cipro) were added to various final concentrations (TCC, TCS: 0.1, 0.33 and 0.5 x MIC; Cipro: 0.1, 0.5 x MIC) and bacteria were incubated for 24 h (or longer if OD_{600} was << 6) at 37°C, 200 rpm. Equivalent amounts of cells (equal to 4 mL OD_{600} = 6) were harvested (6,000 x g, 4°C, 10 min), washed with PBS and either stored at -80°C for later use or directly resuspended in 10 mL 2-propanol 70% (v/v), supplemented with 500 ng/mL menaquinone-9 (MK-9) as internal standard, and sonicated (3 x 30s, 80% intensity, Sonopuls HD 2070 ultrasonic rod, *Bandelin electronic GmbH*) for extraction. Cellular debris was removed by centrifugation (12,000 x g, 30 min, 4°C) and the supernatant was loaded onto a Chromabond® C18 solid phase extraction column (3 mL, 500 mg, *Macherey Nagel*), preconditioned with 6 mL methanol and 6 mL water. Columns were washed with 3 mL water, then 3 mL 2-propanol 70%, and eluted with 10 mL methanol/2-propanol 3:1 (v/v). The eluate was concentrated to dryness and resolved in 200 µL acetonitrile. LC-MS analysis was performed on a *Thermo Fisher Scientific* LTQ-FT Ultra (FT-ICR-MS) coupled with an UltiMate 3000 HPLC system (*Thermo Fisher Scientific*) using atmospheric pressure chemical ionization (APCI). 10 µL of sample was injected into an XBridge BEH300 C4 3.5 µm 2.1 x 150 mm column (*Waters*) and eluted with a gradient of 54% acetonitrile/water, 0.1% FA to 90% acetonitrile/water, 0.1% FA over 1 h at a flow rate of 0.2 mL/min. Single ion monitoring

(SIM) of MK-8 ([M+H], 717.56) and MK-9 ([M+H], 785.62) was performed in parallel and the respective area under the curve (AUC) was determined for quantification using XCalibur software (Thermo Fisher Scientific). AUCs for MK-8 were first normalized to the internal standard MK-9 and then normalized to the DMSO-treated controls.

MenG activity assay. Cellular lysates containing overexpressed MenG were prepared from *S. aureus* pRMC2-MenG as described previously (23). Briefly, cells were grown in B medium with chloramphenicol (10 µg/mL) until OD_{600}~0.5–0.6, induced with anhydrotetracycline (400 ng/mL) and incubated over night. Cells were harvested, washed with PBS, resuspended in 20 mM Tris-HCl, pH 7.5, 1 mM EDTA, 10 mM β-mercaptoethanol, then lysed and adjusted to a final protein concentration of 50 mg/mL.

For the assay, 500 µL of solution containing 100 mM Tris-HCl pH 8, 10 mM $MgCl_2$, 10 mM DTT, 100 µM *S*-adenosyl methionine, 25 µM DMK-2, 200 µL MenG lysate and compounds (TCC, TCS) at different concentrations (5, 25, 50 µM) were incubated at 37°C, 200 rpm, for 80 min. After that, 7 mL 2-propanol 70%, supplemented with 500 ng/mL MK-4 as internal standard, were added and extraction and quantification of menaquinone was performed as for metabolic profiling of MK-8, with the following alterations: 3 mL H_2O was added to the centrifuged supernatant prior to loading onto the solid phase extraction columns and washing of the columns was only conducted with 3 mL H_2O. The gradient of the LC-MS analysis ranged from 18% acetonitrile/water, 0.1% FA to 90% acetonitrile/water, 0.1% FA over 1 h and single ion monitoring was performed for DMK-2 ([M+H], 295.17), MK-2 ([M+H], 309.18) and MK-4 ([M+H], 445.31) in parallel. Resulting data were acquired by three independent experiments.

363 **FabI cloning and activity assay.** FabI was amplified from genomic *S. aureus* DNA
364 using a forward (ggggacaagtttgtacaaaaaagcaggctttATGTTAAATCTTGAAAAC-
365 AAAACA; capital letters indicate overlap with the *fabI* gene) and reverse
366 (ggggaccactttgtacaagaaagctgggtgTTATTTAATTGCGTGGAATCC) primer that
367 introduced AttB sites for Gateway® cloning. The PCR product was cloned into donor
368 vector pDONR201 (*Invitrogen*) by BP reaction, transformed in *E. coli* XL1 blue,
369 reisolated, and a subsequent LR reaction was performed to clone the sequence into
370 pET300/NT-Dest destination vector (*Invitrogen*), giving a FabI construct with an *N*-
371 terminal His tag. This construct was first transformed into *E. coli* XL1 blue, then into *E.*
372 *coli* BL21(DE3) for overexpression. Integrity of the construct was confirmed by Sanger
373 sequencing (*Genewiz*). For expression and purification, mid-exponential phase cultures
374 were induced with 1 mM IPTG and incubated for 4 h at 37 °C, 200 rpm. Cells were
375 harvested, washed with PBS, resuspended in lysis buffer (50 mM Tris pH 8, 300 mM
376 NaCl, 5 mM imidazole), and lysed by sonication (4 x 5 min, 80% intensity, Sonopuls HD
377 2070 ultrasonic rod, *Bandelin electronic GmbH*). Debris was removed by centrifugation
378 (22000 x g, 4°C, 30 min) and the lysate was purified by affinity chromatography on a Ni-
379 NTA agarose column (5 mL column volume, *GE Healthcare*) on an Äkta protein
380 purification system (*GE Healthcare*), using the buffer described above with 20 mM
381 imidazole for washing and 500 mM for elution. After buffer exchange to 50 mM Tris pH
382 8.5, 200 mM NaCl, 2 mM DTT by dialysis, a size exclusion chromatography with a
383 Superdex 200 10/300 GL (120 mL column volume, *GE Healthcare*) was performed for
384 final purification. Protein purity was checked by SDS-PAGE.

385 The substrate *t*-o-NAC thioester was synthesized as described in the literature (28).
386 Conditions for the FabI assay were adapted and modified from the procedure described

387 therein. Briefly, 1.4 µM FabI, 0.8 mM NADPH and compounds at various concentrations
388 (0.1 µM to 100 µM) or DMSO were incubated in 50 mM sodium acetate, pH 6.5, for
389 10 min at 30°C, then *t*-o-NAC thioester (1.6 mM final concentration) was added and the
390 decrease in absorbance at 340 nm was monitored for 30 min at 30°C. Inhibition was
391 determined by the slope of the absorbance curve at t = 0, relative to the DMSO-treated
392 control (100% activity) and the heat control (0% activity, after incubation at 95 °C for 10
393 min). IC_{50} values were determined by fitting to a sigmoidal equation.

394 **Full proteome analysis.** S. aureus NCTC 8325 overnight cultures were diluted into B
395 medium to give a final OD_{600} of 0.1 (40 mL per biological replicate) and then grown
396 (37°C, 200 rpm) for 5 h. Cells were harvested (6,000 x g, 4°C, 10 min), washed with
397 PBS and resuspended in B medium to give a final cell density of 1.5 x 10^9 CFU/mL.
398 10 mL portions were aliquoted into polypropylene plastic tubes and incubated with TCC
399 (0.5 µM, 0.5 x MIC), TCS (0.15 µM, 0.5 x MIC) or DMSO at 37°C, 200 rpm for 1.5 h.
400 Cells were pelleted by centrifugation (6,000 x g, 4°C, 10 min) and washed with PBS.
401 Cells were stored at -80°C for at least 16 h and then lysed. For cell lysis, bacterial cell
402 pellets were resuspended in 200 µL 100 mM Tris pH 7.4 and lysed by sonication (5 x 20
403 s, 65% int. with 30 s rest on ice in between, Sonopuls HD 2070 ultrasonic rod, *Bandelin*
404 *electronic GmbH*). 80 µL of 10% (w/v) SDS and 1.25% (w/v) sodium deoxycholate was
405 added and samples heated for 10 min at 90°C. Lysates were sonicated for 10 s at 10%
406 intensity to shear nucleic acids and centrifuged (13000 x g, RT, 10 min) to pellet debris.
407 Protein concentrations were measured using the Pierce BCA Protein assay kit (*Thermo*
408 *Fisher Scientific, Pierce Biotechnology*) and full proteome samples were adjusted to
409 equal protein amounts. Subsequently, proteins were precipitated with ice-cold acetone

410 (4 volumes) at -20°C overnight, centrifuged (16,900 x g, 4°C, 15 min), and the pellets
411 washed twice with ice-cold methanol (1 mL). Protein pellets were air dried and dissolved
412 in denaturation buffer (7 M urea, 2 M thiourea in 20 mM pH 7.5 HEPES buffer), then
413 reduced with TCEP (10 mM; 37°C, 1,200 rpm, 1 h) and subsequently alkylated with
414 iodoacetamide (12.5 mM; 25°C, 1,200 rpm, 30 min). Alkylation was quenched by the
415 addition of dithiothreitol (12.5 mM) and subsequent incubation (RT, 1,200 rpm, 30 min).
416 For digestion, LysC (1:200 enzyme:protein ratio; 0.5 µg/µL) was added to each sample
417 and the samples incubated at RT with shaking at 700 rpm for 2 h. Following dilution with
418 50 mM TEAB buffer (1:5), samples were further digested with trypsin (1:100
419 enzyme:protein ratio; 0.5 µg/µL) at 37°C overnight. The reaction was stopped by adding
420 FA to a final pH of 2–3. Peptides were desalted on-column using 50 mg SepPak C18
421 Vac cartridges (*Waters*): SepPak C18 cartridges were equilibrated with ACN (1 mL),
422 elution buffer (1 mL; 80% ACN, 0.5% FA) and three times with aqueous 0.5% FA
423 solution (1 mL). Subsequently, the samples were loaded by gravity flow, washed three
424 times with aqueous 0.5% FA solution (1 mL), eluted with elution buffer (0.5 mL, 80%
425 ACN, 0.5% FA) and lyophilized using a vacuum centrifuge.

426 Prior to mass spectrometry peptides were reconstituted in 0.5% (v/v) FA and filtered
427 through 0.22 µm PVDF filters (*Millipore*). Samples were analyzed via HPLC-MS/MS
428 using an UltiMate 3000 nano HPLC system (*Dionex*) equipped with Acclaim C18
429 PepMap100 75 µm ID x 2 cm trap and Acclaim C18 PepMap RSLC, 75 µm ID x 50 cm
430 separation columns coupled to a Q Exactive Plus (*Thermo Fisher Scientific*). Peptides
431 were loaded on the trap column at a flow rate of 5 µL/min with aqueous 0.1% TFA and
432 then transferred onto the separation column at 0.4 µL/min. Buffers for the nano-
433 chromatography pump were aqueous 0.1% FA (buffer A) and 0.1% FA in ACN (buffer

434 B). Samples were separated using a gradient raising buffer B from 5 to 22% in 112 min,
435 followed by a buffer B increase to 32% within 10 min. Buffer B content was further raised
436 to 90% within the next 10 min and held another 10 min at 90%. Subsequently buffer B
437 was decreased to 5% and held until end of the run (total: 152 min). The MS instrument
438 was operated in a TOP12 data dependent mode. MS full scans were performed at a
439 resolution of 140,000 in the orbitrap and the scan range was set from 300 to 1,500 m/z.
440 The AGC target was set to 3.0e6, the maximum ion injection time was 50 ms and
441 internal calibration was performed using the lock mass option. Monoisotopic precursor
442 selection as well as dynamic exclusion (exclusion duration: 60 s) was enabled.
443 Precursors with charge states of >1 and intensities greater than 1.6e4 were selected for
444 fragmentation. Isolation was performed in the quadrupole using a window of 1.6 m/z and
445 an AGC target to 1.0e5 with a maximum injection time of 50 ms. Fragments were
446 generated using higher-energy collisional dissociation (HCD, normalized collision
447 energy: 27%) and detected in the orbitrap.

448 Peptide and protein identifications were performed using MaxQuant (version 1.6.0.1)
449 with Andromeda (39) as search engine using following parameters:
450 Carbamidomethylation of cysteines as fixed and oxidation of methionine as dynamic
451 modifications, trypsin/P as the proteolytic enzyme, 4.5 ppm for precursor mass tolerance
452 (main search ppm) and 0.5 Da for fragment mass tolerance (ITMS MS/MS tolerance).
453 Searches were performed against the Uniprot database for *S. aureus* NCTC 8325
454 (taxon identifier: 93061, downloaded on 19.08.2019). Quantification was performed
455 using MaxQuant's LFQ algorithm (29). The ”I = L“, ”requantify“ and ”match between
456 runs“ (default settings) options were used. Identification was done with at least 2 unique
457 peptides and quantification only with unique peptides. The mass spectrometry

458 proteomics data have been deposited to the ProteomeXchange Consortium via the
459 PRIDE (40) partner repository with the dataset identifier PXD018347.

460 For statistics with Perseus (version 1.6.0.0) (41), four biological replicates were
461 analyzed. Putative contaminants, reverse hits and proteins, identified by side only, were
462 removed. LFQ intensities were $\log_2(x)$ transformed and filtered to contain minimum three
463 valid values in at least one condition. Missing values were imputed on the basis of a
464 normal distribution (width = 0.3, down-shift = 1.8). *P*-values were obtained by a two-
465 sided two sample *t*-test over the four biological replicates.

466 For pathway enrichment analysis using STRING (30), all proteins that showed an
467 $\log_2$(protein enrichment) ratio of compound vs. DMSO-treated control of more than 1 or
468 less than -1 and a $\log_{10}$(*P*-value) > 1 were entered into the database (https://string-
469 db.org/, multiple proteins analysis) and resulting enriched pathways were inspected
470 further.

471 The processed tables for protein group analysis in Perseus and the results of the
472 STRING analysis have been uploaded to the supplementary information as an Excel file
473 (Supplementary Data 2).

Data Availability

The mass spectrometry proteomics data have been deposited to the ProteomeXchange Consortium via the PRIDE (40) partner repository with the dataset identifier PXD018347.

Acknowledgements

R.M. was supported by a doctoral fellowship of the Boehringer Ingelheim Fonds. S.A.S. was funded by the Center for Integrated Protein Science Munich (CIPSM) and Deutsche Forschungsgemeinschaft (DFG). M.W.H. and C.F. were funded by the Federal Ministry for Education and Research (BMBF) under the framework programme 'VIP+' – project 'aBacter'. We thank Philipp Le for critical discussions, Sabrina Schönberger for excellent experimental support, and Mona Wolff, Katja Bäuml, Katja Gliesche and Franziska Erdmann for excellent technical support.

Supplementary Information

The manuscript is supported by two Excel files as supplementary information.

Supplementary Data 1: MIC_{90} raw data and information on tested strains.

(Tab 1) Table of contents of Supplementary Data 1.

(Tab 2) Origin, antibiotic resistance pattern (interpretation according to EUCAST guidelines) and molecular typing results of the clinical *Staphylococcus* strains used in this study.

(Tab 3) Origin, antibiotic resistance pattern and molecular typing results of those clinical *Staphylococcus* strains with intermediate or high level resistance to TCC (MIC ≥ 6.25 µM).

(Tab 4) MIC raw data for all tested *Staphylococcus* strains. Data relate to Fig. 2A.

(Tab 5) Characteristics of the clinical *Enterococcus strains* used in this study.

(Tab 6) MIC raw data for all tested *Enterococcus* strains. Data relate to Fig. 2B.

Supplementary Data 2: Proteomic data table and STRING analysis.

(Tab 1) Table of contents of Supplementary Data 2.

(Tab 2) List of proteins found in the full proteome of *S. aureus* NCTC 8325 after treatment of bacterial cells with DMSO or TCC (0.5 µM), respectively. Average LFQ $\log_2$ fold-change ratios and $-\log_{10}$ *P*-values (*t*-test) are given. Data relate to Fig. 6A.

(Tab 3) List of proteins found in the full proteome of *S. aureus* NCTC 8325 after treatment of bacterial cells with DMSO or TCS (0.15 µM), respectively. Average LFQ $\log_2$ fold-change ratios and $-\log_{10}$ *P*-values (*t*-test) are given. Data relate to Fig. 6B.

(Tab 4) List of proteins that were significantly up- or downregulated ($|\log_2$(protein ratio)$| > 1$ & -log(*P*-value) > 1) by either TCC or TCS treatment. Overlap between both treatments is indicated in yellow. Data relate to Fig. 6C.

(Tab 5) STRING network enrichment analysis for TCC treatment. Proteins that were significantly up- or downregulated ($\log_2$(protein ratio) > 1 or < -1; -log(*P*-value) > 1) by proteomic analysis (see Tab 1 and Tab 3) were entered into the "multiple proteins analysis" tab of the online tool (https://string-db.org/) and the resulting significantly enriched pathways including the network map posted for up- and downregulation separately.

(Tab 6) STRING network enrichment analysis for TCS treatment. Proteins that were significantly up- or downregulated (log_2(protein ratio) > 1 or < -1; -log(*P*-value) > 1) by proteomic analysis (see Tab 2 and Tab 3) were entered into the "multiple proteins analysis" tab of the online tool (https://string-db.org/) and the resulting significantly enriched pathways including the network map posted for up- and downregulation separately.

References

1. MacKenzie AR. 1970. Effectiveness of antibacterial soaps in a healthy population. JAMA 211:973–976.
2. Calafat AM, Ye X, Wong LY, Reidy JA, Needham LL. 2008. Urinary concentrations of triclosan in the U.S. population: 2003–2004. Environ Health Perspect 116:303–307.
3. Schebb NH, Inceoglu B, Ahn KC, Morisseau C, Gee SJ, Hammock BD. 2011. Investigation of human exposure to triclocarban after showering and preliminary evaluation of its biological effects. Environ Sci Technol 45:3109–3115.
4. Christen V, Crettaz P, Oberli-Schrämmli A, Fent K. 2010. Some flame retardants and the antimicrobials triclosan and triclocarban enhance the androgenic activity *in vitro*. Chemosphere 81:1245–1252.
5. Liu JY, Qiu H, Morisseau C, Hwang SH, Tsai HJ, Ulu A, Chiamvimonvat N, Hammock BD. 2011. Inhibition of soluble epoxide hydrolase contributes to the anti-

inflammatory effect of antimicrobial triclocarban in a murine model. Toxicol Appl Pharmacol 255:200–206.

6. Xie W, Zhang W, Ren J, Li W, Zhou L, Cui Y, Chen H, Yu W, Zhuang X, Zhang Z, Shen G, Li H. 2018. Metabonomics indicates inhibition of fatty acid synthesis, beta-oxidation, and tricarboxylic acid cycle in triclocarban-induced cardiac metabolic alterations in male mice. J Agric Food Chem 66:1533–1542.
7. Ajao C, Andersson MA, Teplova VV, Nagy S, Gahmberg CG, Andersson LC, Hautaniemi M, Kakasi B, Roivainen M, Salkinoja-Salonen M. 2015. Mitochondrial toxicity of triclosan on mammalian cells. Toxicol Rep 2:624–637.
8. Teplova VV, Belosludtsev KN, Kruglov AG. 2017. Mechanism of triclosan toxicity: Mitochondrial dysfunction including complex II inhibition, superoxide release and uncoupling of oxidative phosphorylation. Toxicol Lett 275:108–117.
9. Popova LB, Nosikova ES, Kotova EA, Tarasova EO, Nazarov PA, Khailova LS, Balezina OP, Antonenko YN. 2018. Protonophoric action of triclosan causes calcium efflux from mitochondria, plasma membrane depolarization and bursts of miniature end-plate potentials. Biochim Biophys Acta Biomembr 1860:1000–1007.
10. Ying GG, Yu XY, Kookana RS. 2007. Biological degradation of triclocarban and triclosan in a soil under aerobic and anaerobic conditions and comparison with environmental fate modelling. Environ Pollut 150:300–305.
11. Stasinakis AS, Mamais D, Thomaidis NS, Danika E, Gatidou G, Lekkas TD. 2008. Inhibitory effect of triclosan and nonylphenol on respiration rates and ammonia removal in activated sludge systems. Ecotoxicol Environ Saf 70:199–206.
12. Chalew TEA, Halden RU. 2009. Environmental exposure of aquatic and terrestrial biota to triclosan and triclocarban. J Am Water Resour Assoc 45:4–13.

564 13. Dann AB, Hontela A. 2011. Triclosan: environmental exposure, toxicity and
565 mechanisms of action. J of Appl Toxicol 31:285–311.
566 14. Gao L, Yuan T, Cheng P, Bai Q, Zhou C, Ao J, Wang W, Zhang H. 2015. Effects of
567 triclosan and triclocarban on the growth inhibition, cell viability, genotoxicity and
568 multixenobiotic resistance responses of *Tetrahymena thermophila*. Chemosphere
569 139:434–440.
570 15. Hedrick-Hopper TL, Koster LP, Diamond SL. 2015. Accumulation of triclosan from
571 diet and its neuroendocrine effects in Atlantic croaker (*Micropogonias undulatus*)
572 under two temperature regimes. Mar Environ Res 112:52–60.
573 16. McMurry LM, Oethinger M, Levy SB. 1998. Triclosan targets lipid synthesis. Nature
574 394:531–532.
575 17. Heath RJ, Yu YT, Shapiro MA, Olson E, Rock CO. 1998. Broad spectrum
576 antimicrobial biocides target the FabI component of fatty acid synthesis. J Biol
577 Chem 273:30316–30320.
578 18. Heath RJ, Li J, Roland GE, Rock CO. 2000. Inhibition of the *Staphylococcus aureus*
579 NADPH-dependent enoyl-acyl carrier protein reductase by triclosan and
580 hexachlorophene. J Biol Chem 275:4654–4659.
581 19. Villalain J, Mateo CR, Aranda FJ, Shapiro S, Micol V. 2001. Membranotropic effects
582 of the antibacterial agent triclosan. Arch Biochem Biophys 390:128–136.
583 20. Walsh SE, Maillard JY, Russell AD, Catrenich CE, Charbonneau DL, Bartolo RG.
584 2003. Activity and mechanisms of action of selected biocidal agents on gram-
585 positive and -negative bacteria. J Appl Microbiol 94:240–247.
586 21. Orsi M, Noro MG, Essex JW. 2011. Dual-resolution molecular dynamics simulation
587 of antimicrobials in biomembranes. J R Soc Interface 8:826–841.

22. Pujol E, Blanco-Cabra N, Julián E, Leiva R, Torrents E, Vázquez S. 2018. Pentafluorosulfanyl-containing triclocarban analogs with potent antimicrobial activity. Molecules 23:2853.

23. Le P, Kunold E, Macsics R, Rox K, Jennings MC, Ugur I, Reinecke M, Chaves-Moreno D, Hackl MW, Fetzer C, Mandl FAM, Lehmann J, Korotkov VS, Hacker SM, Kuster B, Antes I, Pieper DH, Rohde M, Wuest WM, Medina E, Sieber SA. 2020. Repurposing human kinase inhibitors to create an antibiotic active against drug-resistant *Staphylococcus aureus*, persisters and biofilms. Nat Chem 12:145–158.

24. Walsh S, Maillard JY, Russell A, Catrenich C, Charbonneau D, Bartolo R. 2003. Development of bacterial resistance to several biocides and effects on antibiotic susceptibility. J Hosp Infect 55:98–107.

25. Schulte B, Bierbaum G, Pohl K, Goerke C, Wolz C. 2013. Diversification of clonal complex 5 methicillin-resistant *Staphylococcus aureus* strains (Rhine-Hesse clone) within Germany. J Clin Microbiol 51:212–216.

26. Engelthaler DM, Kelley E, Driebe EM, Bowers J, Eberhard CF, Trujillo J, Decruyenaere F, Schupp JM, Mossong J, Keim P, Even J. 2013. Rapid and robust phylotyping of spa t003, a dominant MRSA clone in Luxembourg and other European countries. BMC Infect Dis 13:339.

27. Gravel J, Paradis-Bleau C, Schmitzer AR. 2017. Adaptation of a bacterial membrane permeabilization assay for quantitative evaluation of benzalkonium chloride as a membrane-disrupting agent. Med Chem Commun 8:1408–1413.

28. Zheng CJ, Yoo JS, Lee TG, Cho HY, Kim YH, Kim WG. 2005. Fatty acid synthesis is a target for antibacterial activity of unsaturated fatty acids. FEBS Lett 579:5157–5162.

612 29. Cox J, Hein MY, Luber CA, Paron I, Nagaraj N, Mann M. 2014. Accurate proteome-
613 wide label-free quantification by delayed normalization and maximal peptide ratio
614 extraction, termed MaxLFQ. Mol Cell Proteomics 13:2513–2526.
615 30. Szklarczyk D, Gable AL, Lyon D, Junge A, Wyder S, Huerta-Cepas J, Simonovic M,
616 Doncheva NT, Morris JH, Bork P, Jensen LJ, Mering C. 2019. STRING v11:
617 protein–protein association networks with increased coverage, supporting functional
618 discovery in genome-wide experimental datasets. Nucleic Acids Res 47:D607–
619 D613.
620 31. Makhlin J, Kofman T, Borovok I, Kohler C, Engelmann S, Cohen G, Aharonowitz Y.
621 2007. *Staphylococcus aureus* ArcR controls expression of the arginine deiminase
622 operon. J Bacteriol 189:5976–5986.
623 32. Ashburner M, Ball CA, Blake JA, Botstein D, Butler H, Cherry JM, Davis AP,
624 Dolinski K, Dwight SS, Eppig JT, Harris MA, Hill DP, Issel-Tarver L, Kasarskis A,
625 Lewis S, Matese JC, Richardson JE, Ringwald M, Rubin GM, Sherlock G. 2000.
626 Gene ontology: tool for the unification of biology. Nat Genet 25:25–29.
627 33. The Gene Ontology Consortium. 2018. The Gene Ontology Resource: 20 years and
628 still going strong. Nucleic Acids Res 47:D330–D338.
629 34. El-Gebali S, Mistry J, Bateman A, Eddy SR, Luciani A, Potter SC, Qureshi M,
630 Richardson LJ, Salazar GA, Smart A, Sonnhammer ELL, Hirsh L, Paladin L,
631 Piovesan D, Tosatto SCE, Finn RD. 2019. The Pfam protein families database in
632 2019. Nucleic Acids Res 47:D427–D432.
633 35. Diep BA, Gill SR, Chang RF, Phan TH, Chen JH, Davidson MG, Lin F, Lin J,
634 Carleton HA, Mongodin EF, Sensabaugh GF, Perdreau-Remington F. 2006.

635 Complete genome sequence of USA300, an epidemic clone of community-acquired
636 meticillin-resistant *Staphylococcus aureus*. Lancet 367:731–739.
637 36. Brenwald NP, Fraise AP. 2003. Triclosan resistance in methicillin-resistant
638 *Staphylococcus aureus* (MRSA). J Hosp Infect 55:141–144.
639 37. McDonnell G, Pretzer D. 1998. Action and targets of triclosan. ASM News 64:670–
640 674.
641 38. Rao CV S, Bockstael K, Nath S, Engelborghs Y, Anné J, Geukens N. 2009.
642 Enzymatic investigation of the *Staphylococcus aureus* type I signal peptidase SpsB
643 – implications for the search for novel antibiotics. FEBS J 276:3222–3234.
644 39. Cox J, Mann M. 2008. MaxQuant enables high peptide identification rates,
645 individualized p.p.b.-range mass accuracies and proteome-wide protein
646 quantification. Nat Biotechnol 26:1367–1372.
647 40. Perez-Riverol Y, Csordas A, Bai J, Bernal-Llinares M, Hewapathirana S, Kundu DJ,
648 Inuganti A, Griss J, Mayer G, Eisenacher M, Perez E, Uszkoreit J, Pfeuffer J,
649 Sachsenberg T, Yilmaz S, Tiwary S, Cox J, Audain E, Walzer M, Jarnuczak AF,
650 Ternent T, Brazma A, Vizcaino JA. 2019. The PRIDE database and related tools
651 and resources in 2019: improving support for quantification data. Nucleic Acids Res
652 47:D442–D450.
653 41. Tyanova S, Temu T, Sinitcyn P, Carlson A, Hein MY, Geiger T, Mann M, Cox J.
654 2016. The Perseus computational platform for comprehensive analysis of
655 (prote)omics data. Nat Methods 13:731–740.

656 **Figures**

657

658 **Figure 1** – Structures of the antibacterial agents triclocarban (TCC) and triclosan (TCS),
659 structurally related PK150, and sorafenib (SFN). Their respective activities (minimal
660 inhibitory concentrations) in *S. aureus* NCTC 8325 are displayed below.

661

662 **Figure 2** – **TCC exhibits a different activity spectrum compared to PK150.** MIC
663 determination of PK150 and TCC against a panel of 100 strains of staphylococci **(A)** and
664 enterococci **(B)**. MICs were tested up to a concentration of 25 µM and the distribution
665 plotted for each compound. Dotted lines indicate the respective MIC_{90} value, i.e. the
666 concentration at which the growth of 90% of tested strains was inhibited. Experiments
667 were performed in two biologically independent replicates, and for cases in which the
668 MIC differed between the replicates the higher value was taken as resulting MIC. See
669 Supplementary Data 1 for further details.

670

671 **Figure 3** – **Effects on membrane integrity and SpsB activation potential by TCC,**
672 **TCS and PK150. (A)** Membrane integrity assay analyzing the permeability of *S. aureus*
673 NCTC 8325 cells upon treatment with TCC, TCS, PK150 or positive control
674 benzalkonium chloride (BAC). Interaction of propidium iodide with DNA was measured
675 over time. Data are representative for three biological replicates. **(B)** FRET-based SpsB
676 activity assay with membrane-bound endogenous SpsB from *S. aureus* NCTC 8325
677 (200 µg/mL total protein concentration) and different concentrations of TCC, TCS, and
678 PK150 (positive control). Substrate cleavage rates are normalized to DMSO-treated

679 samples. Data represent mean values ± s.d. of averaged triplicates of *n* = 4 biologically
680 independent experiments.

681 **Figure 4** – **Interference with menaquinone biosynthesis and inhibition of MenG by**
682 **TCC and TCS. (A)** MIC shift by addition of menaquinone-4 (MK-4) to the bacterial
683 growth medium. MICs of TCC and TCS were determined in the presence of various
684 concentrations of MK-4 as indicated. The data represent results from three biologically
685 independent experiments performed in triplicates. Where the MIC varied between
686 replicates, the MIC is given as a range as displayed by the extension of the data point.
687 **(B)** Metabolic profiling of endogenous menaquinone levels in *S. aureus* NCTC 8325
688 cells on compound treatment. Bacteria were treated with sub-inhibitory concentrations
689 (0.1-fold to 0.5-fold of the respective MIC) of TCC, TCS, or ciprofloxacin (Cipro) and
690 menaquinone-8 (MK-8) was extracted and quantified by LC–MS. MK-8 levels are
691 normalized to DMSO-treated samples. Each color represents an individual, independent
692 extraction experiment, where differently shaped symbols (circles, rectangles, triangles
693 and diamonds) indicate independent biological samples. Error bars denote mean values
694 ± s.d. **(C)** Enzymatic assay monitoring the methylation of DMK-2 by cellular lysate of
695 MenG-overexpressing *S. aureus* pRMC2-MenG (20 mg/ml total protein concentration).
696 Production of MK-2 was quantified by LC–MS and normalized to the respective DMSO-
697 treated samples. Data represent the averaged values ± s.d. from three independent
698 experiments.

699

700 **Figure 5** – **Inhibition of FabI by TCC, TCS and PK150.** Recombinant FabI was pre-
701 incubated with NADPH and compounds at different concentrations, then the substrate *t*-
702 o-NAC thioester was added and the decrease in absorbance at 340 nm was recorded.

703 Enzyme activity was determined by the slope at $t = 0$ and relative activity was calculated
704 by normalization to the DMSO-treated control (100% activity) and the heat-inactivated
705 negative control (0% activity). The data were subsequently fitted to a sigmoidal
706 equation. For TCS the IC_{50} was calculated to be 3.76 ± 0.11 µM. Data represent mean
707 values ± s.d. of averaged triplicates from three independent experiments.
708
709 **Figure 6 – Full proteome analysis of *S. aureus* NCTC 8325 upon TCC and TCS**
710 **treatment. (A,B)** Volcano plots showing the $\log_2$-fold change of protein levels in the full
711 proteome of *S. aureus* treated with sub-inhibitory concentrations (0.5 x MIC) of TCC (**A**)
712 or TCS (**B**). Colors denote pathways that were significantly enriched among
713 downregulated proteins ($\log_2$(protein ratio) < −1 & -log(*P*-value) > 1) by STRING (30)
714 analysis. Blue dots represent the proteins associated with the arginine deiminase (ADI)
715 pathway (see below) which were affected by TCC treatment. Green and brown dots
716 represent proteins associated with the EIIB/EIIC phosphotransferase system and ABC
717 transporter transmembrane domains, respectively. These terms were found to be
718 enriched in the STRING analysis of TCS treatment. Pink circles represent all proteins –
719 regardless of *P*-value – which were up- or downregulated (|$\log_2$(protein ratio)| > 1) by
720 both TCC and TCS treatment . The only protein also meeting the significance cut-off (-
721 log(*P*-value) > 1) is shown in green (PTS system EIIBC component, Q2G1G5).The data
722 represent average values and the *P*-values were calculated using a two-sided two-
723 sample *t*-test; $n = 4$ independent experiments per group. See Supplementary Data 2 for
724 further details. **(C)** Venn diagram showing overlap in protein up- or downregulation
725 between TCC and TCS treatment. The respective circles indicate the total number of
726 proteins for each stated case (|$\log_2$(protein ratio)| > 1 & -log(*P*-value) > 1) **(D)** Table

identifying proteins associated with the ADI pathway (31) in the volcano plots in panels **(A)** and **(B)**. All proteins are annotated within the KEGG pathway ”arginine biosynthesis“. **(1)**, **(3)**, and **(4)** are directly annotated as elements of the ADI pathway in *S. aureus* NCTC 8325 by GO (33). **(2)** is located in the same gene cluster as **(1)** and its homologs in related *S. aureus* strains (such as COL, MW2 or USA300) are annotated as part of the ADI pathway in Uniprot. **(5)** catalyzes the same reaction as **(2)**, but according to its annotation seems to be involved in arginine biosynthesis rather than catabolism.

	Triclocarban (TCC)	**Triclosan (TCS)**	**PK150**	**Sorafenib (SFN)**
MIC in *S. aureus* NCTC 8325	1 µM	0.3-0.5 µM	0.3 µM	3 µM

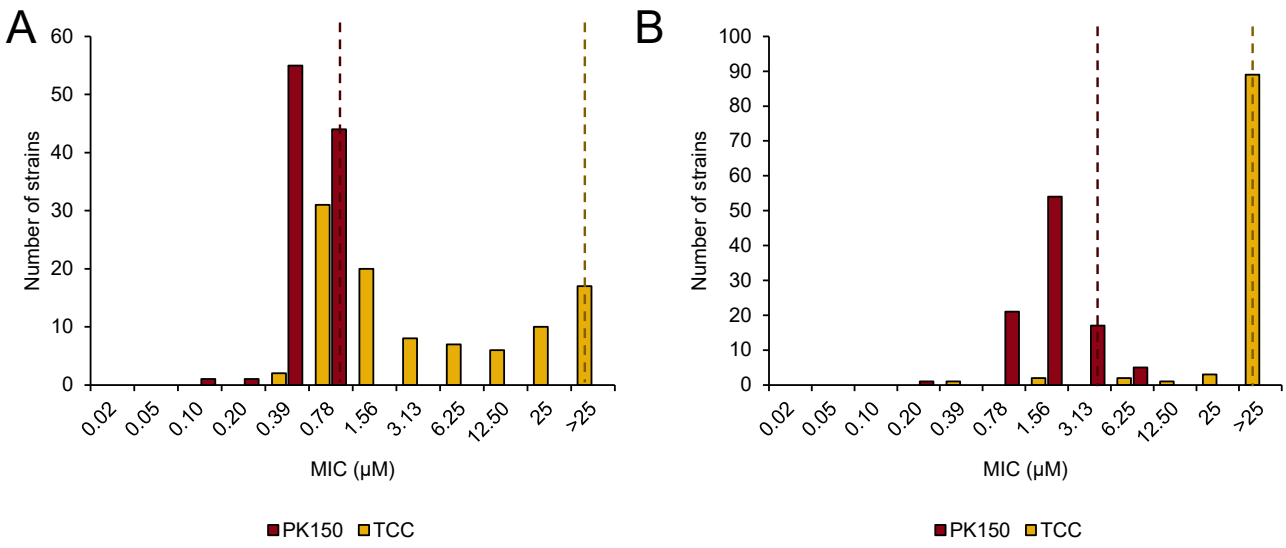

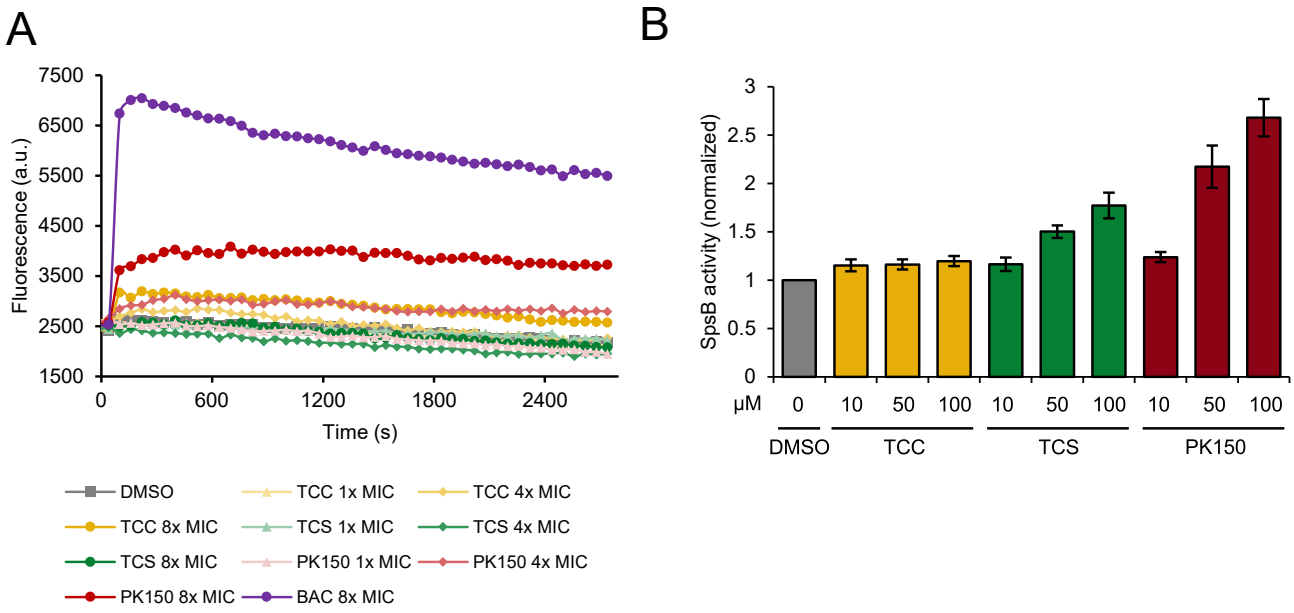

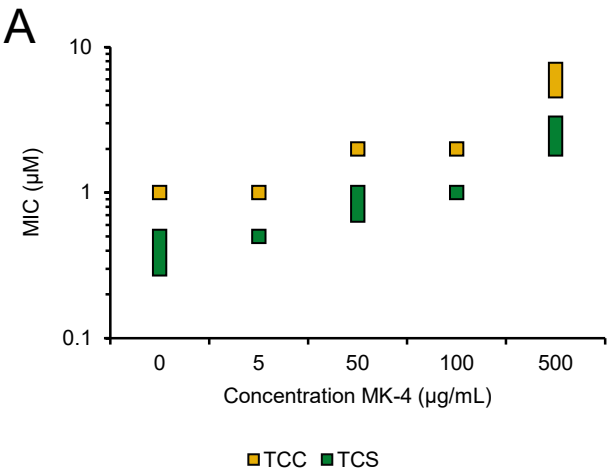

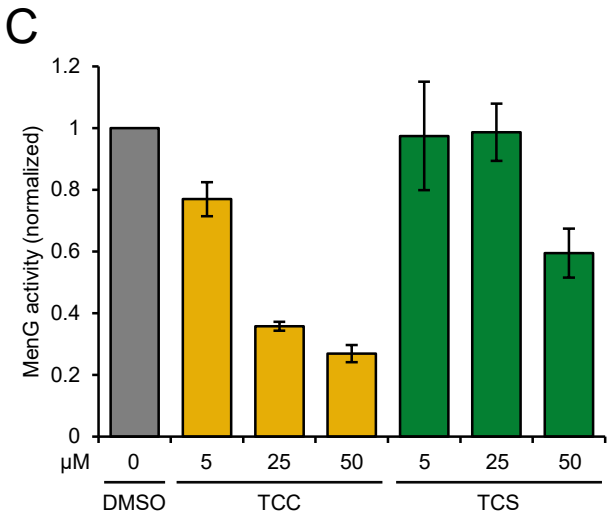

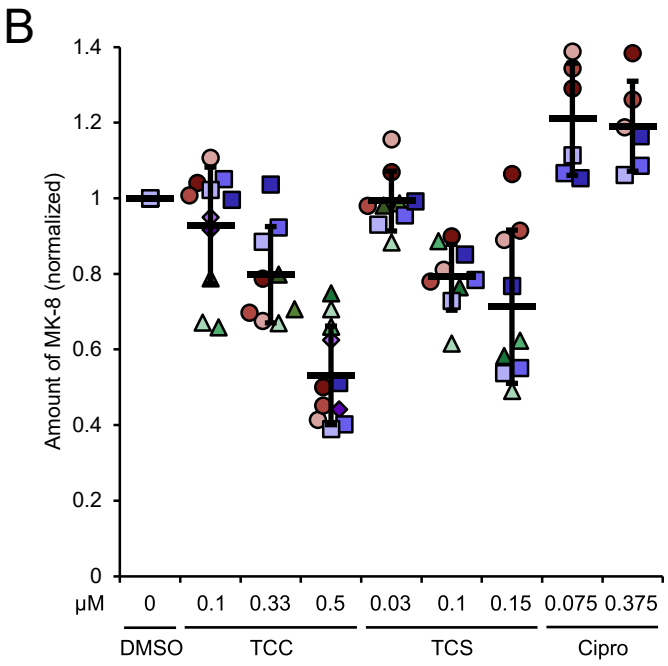

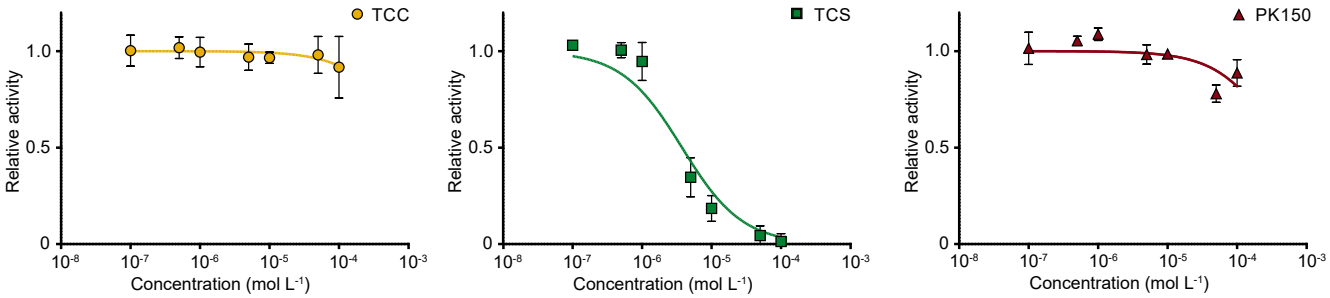

A

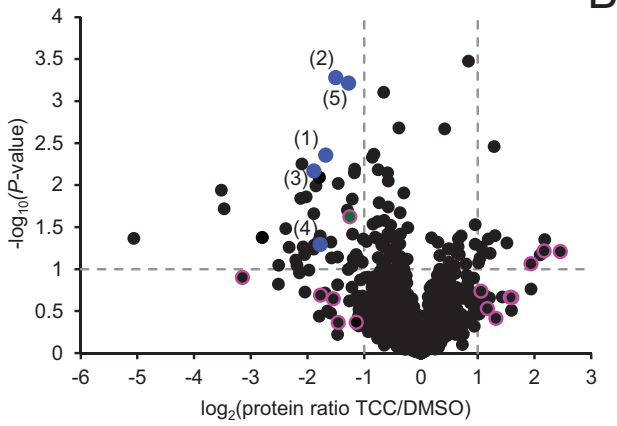

B

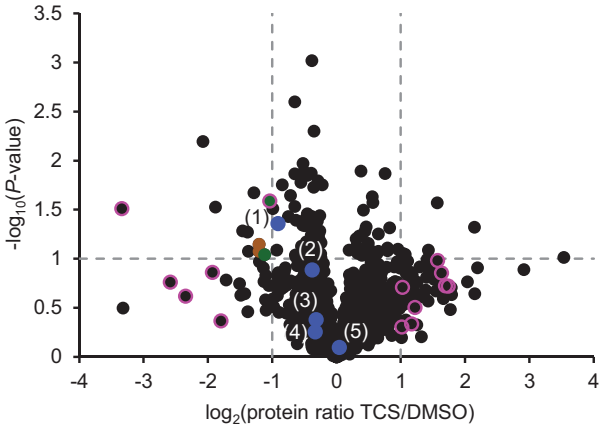

C

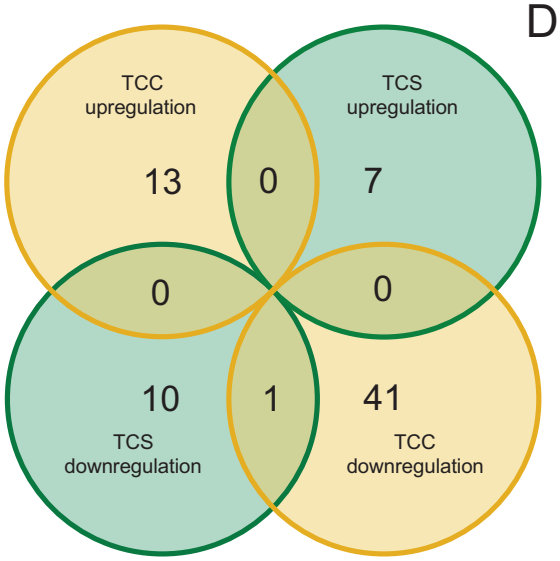

D

	Gene	Protein name	UniProt ID
(1)	*arcA*	arginine deiminase	Q2FUX7
(2)	*arcB/argF*	ornithine carbamoyltransferase	Q2FUX8
(3)	*arcC1*	carbamate kinase 1	Q2FZA9
(4)	*arcC2*	carbamate kinase 2	Q7X2S2
(5)	*argF*	ornithine carbamoyltransferase	Q2FZB0